RESEARCH ARTICLE

The variability of the sediment plume and ocean circulation features of the Nass River Estuary, British Columbia

David B. Fissel*, Yuehua Lin, Alison Scoon, Jose Lim, Leslie Brown and Ryan Clouston

ASL Environmental Sciences, Victoria, BC, Canada

Abstract: The Nass River discharges into Nass Bay and Iceberg Bay, which are adjoining tidal inlets located within the northern inland waters of British Columbia, Canada. After the Skeena River, the Nass River is the second longest river within northern British Columbia, which discharges directly into Canadian waters of the Pacific Ocean. It is also supports one of the most productive salmon fisheries in northern British Columbia. The Nass River discharges into the eastern end of Nass Bay. Nass Bay, in turn feeds into Portland Canal and the fresh surface waters then flows westward to the Pacific Ocean *via* Dixon Entrance. The tides in Northern British Columbia are very large with a tidal height range of just over 7 m. Nass Bay is a shallow inlet of less than 10 km in length with typical water depths of than 10 m or less. The existing knowledge of oceanographic processes in Nass and Iceberg Bays was rudimentary until three years ago, when the first modern oceanographic measurements were obtained. In this study, the seasonal and tidal variability of the lateral extent of the Nass River surface plume is mapped from analyses of Landsat satellite data spanning the period from 2008 to 2015. A high resolution coupled three dimensional (3D) hydrodynamic model was developed and implemented, within the widely used and accepted Delft3D modeling framework, which was forced and validated using recent 2013–2016 *in-situ* oceanographic measurements. The combined satellite and numerical modeling methods are used to study the physical oceanographic and sediment transport regime of Nass and Iceberg Bays and the adjoining waters of Portland Inlet and Observatory Inlet. The ocean circulation of Nass and Iceberg Bays was found to be dominated by tidal currents, and by the highly seasonal and variable Nass River freshwater discharges. Complex lateral spatial patterns in the tidal currents occur due to the opening of the southwestern side of Nass Bay onto the deeper adjoining waters of Iceberg Bay. Surface winds are limited to a secondary role in the circulation variability. The sediment dynamics of the Nass Bay system features a very prominent surface sediment plume present from the time of freshet in mid-spring through to large rainfall runoff events in the fall. The time-varying turbidity distribution and transport paths of the Nass River sediment discharges in the study area were characterized using the model results combined with an analysis of several high-resolution multi-year Landsat satellite data sets.

Keywords: Nass Bay; Nass River; iceberg bay; observatory inlet; Portland Inlet; circulation; numerical model; tidal current; wind-driven current; stratification; landsat satellite; remote sensing

*Correspondence to: David B. Fissel, ASL Environmental Sciences, #1-6703 Rajpur Place, Victoria, BC, Canada; V8M 1Z5; Email: dfissel@aslenv.com

Received: October 16, 2017; **Accepted:** December 12, 2017; **Published Online:** December 28, 2017

Citation: Fissel D B, Lin Y, Scoon A, *et al*. (2017). The variability of the sediment plume and ocean circulation features of the Nass River Estuary, British Columbia. *Satellite Oceanography and Meteorology*, 2(2): 316. http://dx.doi.org/10.18063/SOM.v2i2.316

1. Introduction

The Nass River is one of the longest rivers in northern British Columbia (BC) draining into the Pacific Waters of BC. It is also supports one of the most productive salmon fisheries of northern British Columbia (Sierra Club of Canada, 2006). The Nass River basin represents the territory of the Nisga'a First Nation, for which the first modern-day treaty settlement

in British Columbia was achieved taking effect in the year 2000 (McKee, 2009).

The objective of this study is to provide improved understandings of the physical oceanography of the Nass Estuary based on recent oceanographic measurements and satellite imagery and the use of an advanced hydrodynamic numerical model.

1.1 Physical Setting

The geography of the study area is complex. The northern inland waters of British Columbia are characterized by a myriad of inlets and fjords entering into the inland seas of Dixon Entrance and Hecate Strait (Figure 1A). The Nass River estuary starts at the eastern end of Nass Bay at the mouth of the Nass River and extends to adjoining Portland Inlet (Figure 1B). Freshwater discharges dominate the physical oceanography of Nass Bay; as well these freshwater discharges extend into the adjoining waters of Iceberg Bay and Portland Inlet (Figure 1B). Previously, investigations of the oceanography of this remote area of northern British Columbia have been very limited. Nass Bay opens onto the Portland Inlet system which extends as Observatory Inlet past the entrance to Nass Bay. These fjord waters are characterized as long features spanning distances of 100 km or more, with deep waters of up to 600 m, and shallow sills separating the water bodies into discrete basins. There is a shallow sill in Observatory Inlet of 30 m depth just to the northeast of the entrance to Nass Bay (Figure 2A). The Nass Bay and Iceberg Bay system is much smaller than the typical fjords and inlets of the area. Its length is only about 10 km from the mouth to the eastern part of Nass Bay where the Nass River waters enter. The lateral extent of about 12 km is unusually wide, making up western Nass Bay and its appendage, Iceberg Bay. Nass Bay is shallow, typically less than 10 m above low tide, due to the deposition of river sediments in this area which are exposed as extensive tidal flats at low tides. Water depths exceeding 20 m are confined to Iceberg Bay which extends down to 80 m depth and along the western part of the entrance to the Bay. There is also a narrow trough extending into Nass Harbor separating Nass Bay from Iceberg Bay (Figure 2B).

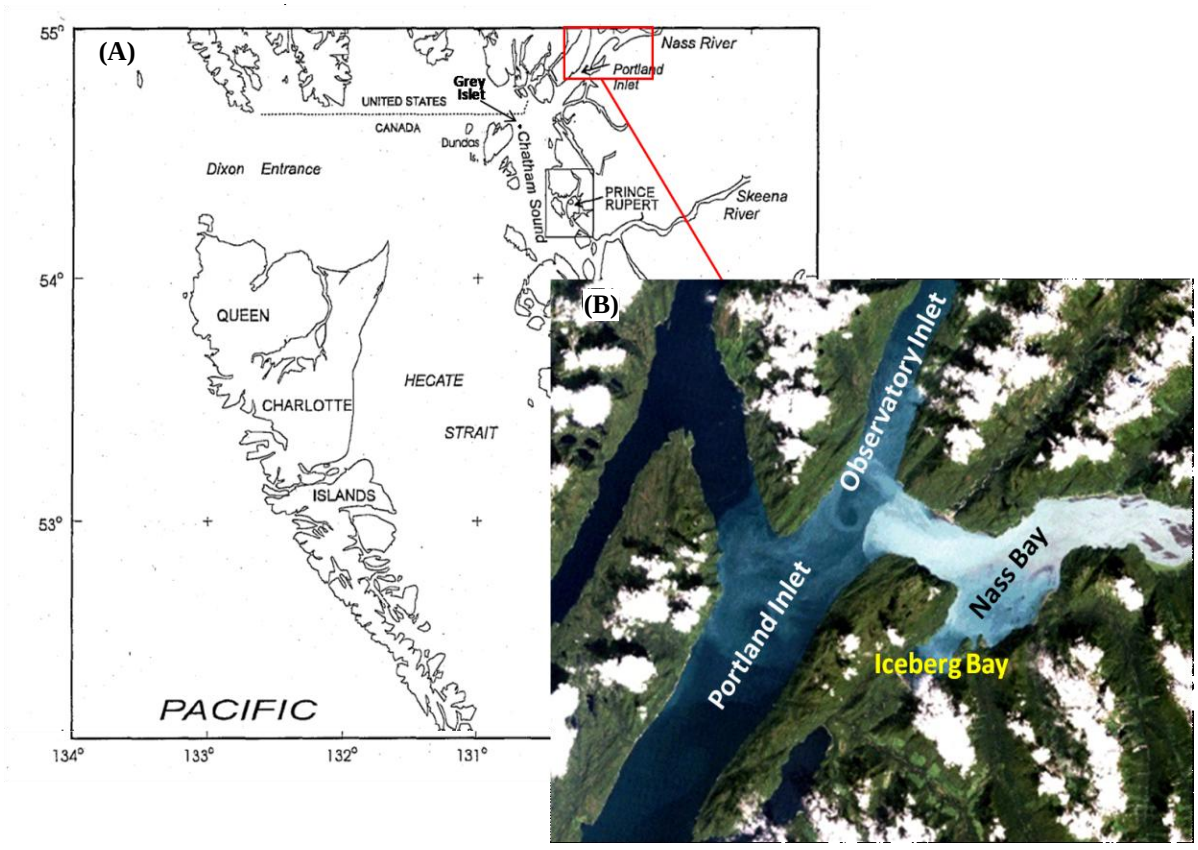

Figure 1. (**A**) The inland waterways of northern British Columbia; (**B**) The major waterways of the study area as a Landsat 8 image from 7th August 2011. The satellite image data is enhanced to show the turbid waters of the Nass River plume as the lighter color shading in Nass and Iceberg Bays. The Nass River estuary consists of Nass Bay and Iceberg Bay.

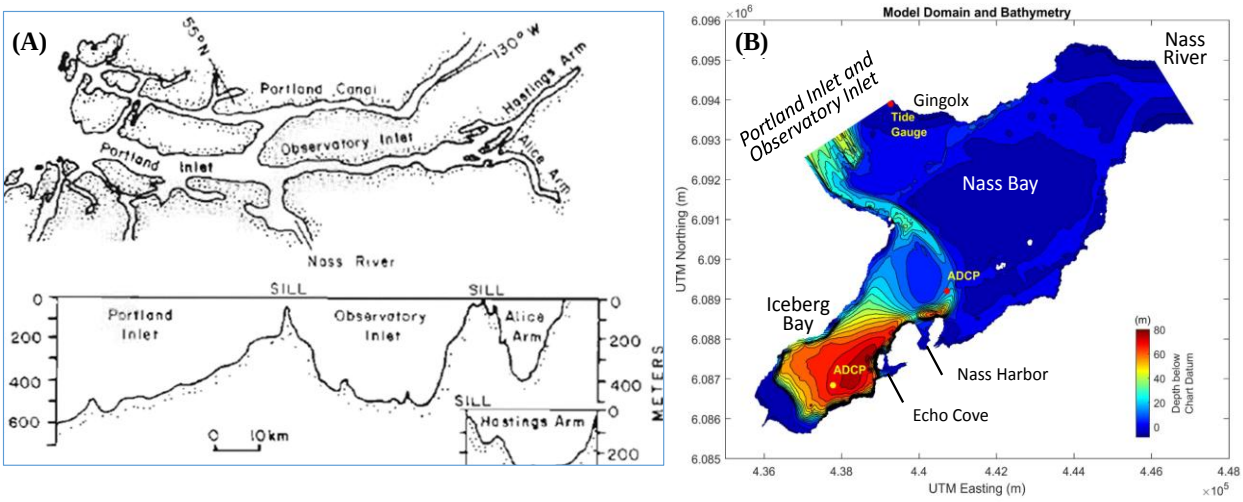

Figure 2. The bathymetry of the study area: (**A**) the channel depth of Portland Inlet and Observatory Inlet (after Pickard, 1961) and (**B**) the water depths of Nass Bay and Iceberg Bay as derived from the Canadian Hydrographic Service Chart No. 3920

1.2 Nass River

The Nass River originates in the interior of British Columbia in the Skeena Mountains and flows southwestward over a distance of approximately 400 km into Nass Bay. The total drainage area is approximately 25,000 km^2 and the average annual discharge is 780 m^3/s, computed from the long-term discharge measurements, from 1930 to the present, by the Water Survey of Canada at the "Nass River above Shumal Creek" gauge. The Nass River is the second longest river within northern British Columbia, which discharges directly into Canadian waters of the Pacific Ocean, after the Skeena River. The Nass River discharges are characterized by a pronounced annual cycle with average values increasing quickly from late April until freshet in late May to early June with typical values of 2200 m^3/s (Figure 3). The discharges decrease gradually through the summer and fall seasons, although large episodic values due to intense weather systems associated with high rainfall can occur in September and October, with peak daily values of up to 6000 m^3/s. By November, precipitation from weather systems is increasingly in the form of snow rather than rain with the result that the Nass River discharges decrease to much lower values (125–175 m^3/s) in winter and early spring.

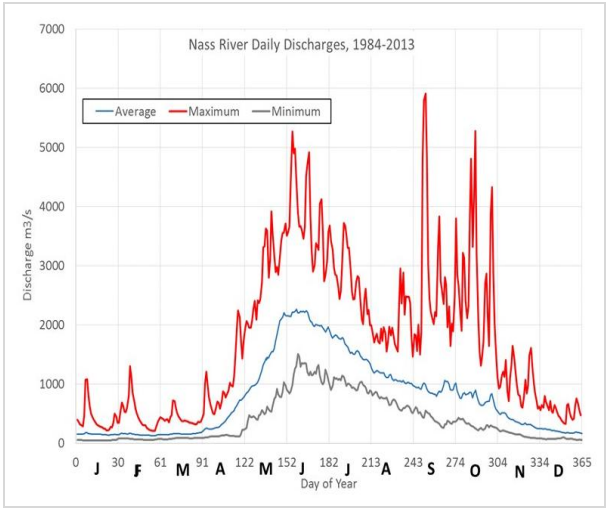

Figure 3. The daily Nass River discharges as measured by the Water Survey of Canada for the 30 year period of 1984–2013, displayed as the daily mean discharge and the minimum and maximum discharge values recorded on each day of the year.

2. Previous Oceanographic Studies

The oceanography of the extensive network of fjords and inlets in the northern waters of British Columbia has been studied starting with the first ocean research cruise to Portland Inlet and Observatory Inlet in 1951 (Pickard, 1961). Regular oceanographic cruises to the extended area of this study occurred from 1977 through the early 1980's which have been documented in Birch *et al.* (1985). The physical oceanography of Observatory Inlet through to its headwaters in Alice Arm were addressed in ocean research papers (Farmer and Denton, 1985; Stacey and Zedel, 1986) and in environmental assessment technical reports (Krauel, 1981). However, these studies did not extend into Nass and Iceberg Bays. Water level data were collected at the entrance to Nass Bay in 1963 and 1966 by the Canadian Hydrographic Service and ocean wave measurements were collected off the mouth of Nass Bay from 1977–1978 (Birch *et al.*, 1985). The first integrated oceanographic measurement

program in Nass and Iceberg Bays was conducted as part of the present study with data collection in 2013 (currents and water levels) and at quarterly intervals for the period of mid-2015 to mid-2016 (currents, water levels, temperature, salinity and turbidity).

3. The Large Scale Distribution of the Nass River Plume from Satellite Remote Sensing

Landsat satellite imagery was reviewed over a ten-year period (2006–2015) for use in mapping the horizontal distribution of the Nass River plume at the surface. The satellite data sets (USGS, 2016, 2017) were obtained for the months April to November and a wide range of tidal and Nass River freshwater discharge conditions. Landsat 8 Operational Land Imager (OLI) and Landsat 5 Thematic Mapper (TM) data were used. These sensors provide 30 m × 30 m pixels which are demonstrated to have sufficiently high spatial and radiometric resolution to clearly resolve the spatial extent and variability of the Nass River plume. The images were found to be of high quality in that they provided many cloud-free images of Nass and Iceberg Bays.

All Landsat data were downloaded from the USGS Glovis website (https://glovis.usgs.gov/) as standard level 1T products (radiometrically calibrated and orthocorrected). Of the original 27 data sets obtained for the years 2006 to 2015, fifteen images, from the years 2008–2015, were selected for processing to Top-of-Atmosphere (TOA) reflectance. Calibration to TOA reflectance provides a radiometric normalization that accounts for temporal variations in sun-earth geometry. The coefficients for the Landsat imagery data are provided by the National Aeronautics and Space Administration (NASA), and these corrections were applied to the satellite data using ENVI version 5.3 software (Exelis Visual Information Solutions, Boulder, CO). Additional correction to compensate for the effects of atmospheric absorption and scattering were not applied.

For the images in Figure 4, a water turbidity index, WT-2, was calculated from the Landsat 8 TOA reflectance data by subtracting the 865 nanometer band (near infrared) from the 655 nanometer band (red). In previous unpublished work, we have found good correlation between the WT-2 index with *in situ* surface turbidity measurements. These findings are supported by the use of reflectance in the red spectral range which has been applied by many authors to map surface turbidity (*e.g.*, Miller *et al.*, 2004, Chen *et al.*, 2007, Gholizadeh *et al.*, 2016, Constantin *et al.*, 2016, Quang *et al.*, 2017). Subtraction of the signal in the near infrared band is used to correct for specular reflection at the surface of the water, known as sun-glint.

The spatial distribution of the Nass River plume in Nass Bay and Iceberg Bay exhibits differences between the ebb and flood tide during large Nass River discharges near the time of river freshet in early June 2014 (Figure 4). As the ebb tide is ending, the Nass River sediment plume spans nearly all of Nass Bay and the northeastern half of Iceberg Bay with large reflectance values indicative of higher surface turbidity (Figure 4A). At the end of the flood tide, the high reflectance values of the sediment plume are confined to the western portion of Nass Bay where the Nass River waters enter Nass Bay, and in the northern half of the entrance to Nass Bay (Figure 4B). In the southern part of the entrance, much

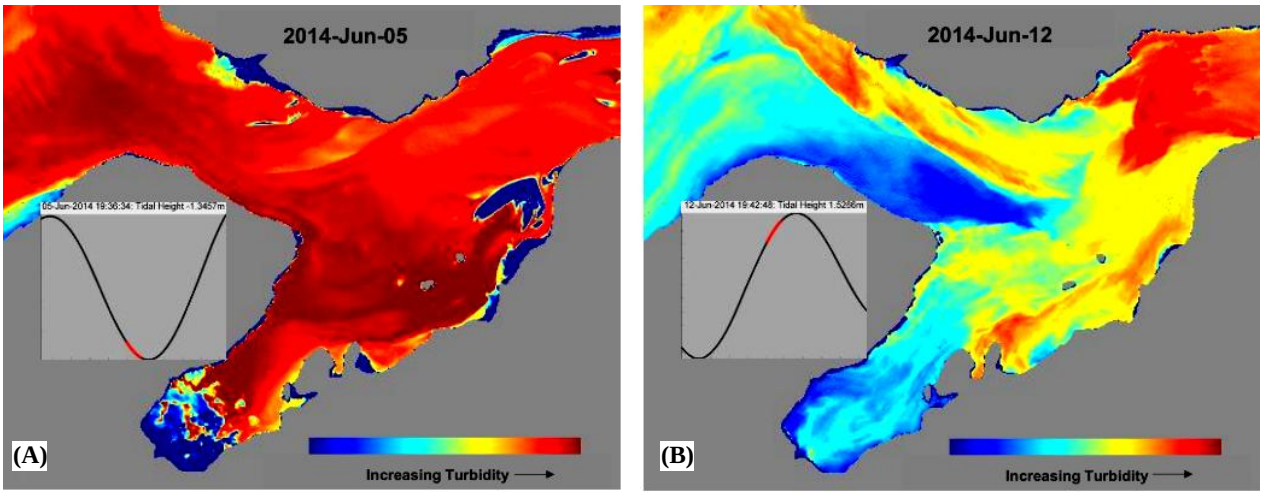

Figure 4. Landsat satellite imagery scenes of the Nass River plume during freshet in June 2014 (**A**) at low water following an ebb tide and (**B**) at high water following a flood tide. Uniform enhancements have been applied to these Landsat 8 imagery data so that the surface reflectance values, indicative of turbidity, are comparable in each image scene.

clearer waters occur as the flood tide carries the offshore waters from the comparatively clearer waters of Portland Inlet into Nass Bay. Moderate levels of reflectance values are observed in southwestern Nass Bay while Iceberg Bay has low reflectance values.

Over the larger area of Nass and Iceberg Bays, and Portland and Observatory Inlets, selected Landsat images (Figure 5 and Figure 6) were processed to TOA reflectance as described above. These figures show true colour (RGB) composites of the Landsat red, green and blue bands, with a consistent linear enhancement applied across all images. As such the images can be considered to be directly comparable in terms of the displayed colours presented. The images show that the freshwater input from the Nass River is dominated by suspended sediments which are represented by a near-white colour (Figure 5 and Figure 6). The saline sea water has a much weaker return and is represented by the darker colour. The Landsat imagery-derived spatial distribution of the Nass River plume enables its flow characteristics and transport paths to be easily identified throughout the tidal cycle. Beyond the distinct Nass River plume, there are areas in which lower concentrations of suspended sediments from the Nass River are mixed with saline sea water represented by areas of intermediate brightness with small-scale horizontal patterns present.

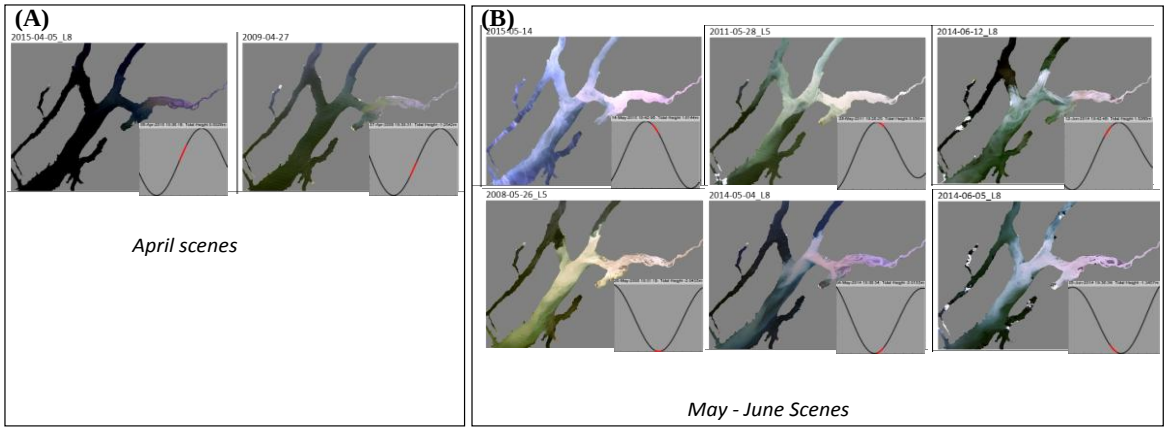

Figure 5. Landsat satellite imagery scenes of the Nass River plume (**A**) for April with low Nass River discharges and (**B**) for May–June with moderate to high river discharges for various years from 2008 to 2015. These RGB thumbnail images are uniformly enhanced using identical look-up tables. The top row of images are scenes during a flood tide and the bottom row of images are scenes during an ebb tide or at low water levels.

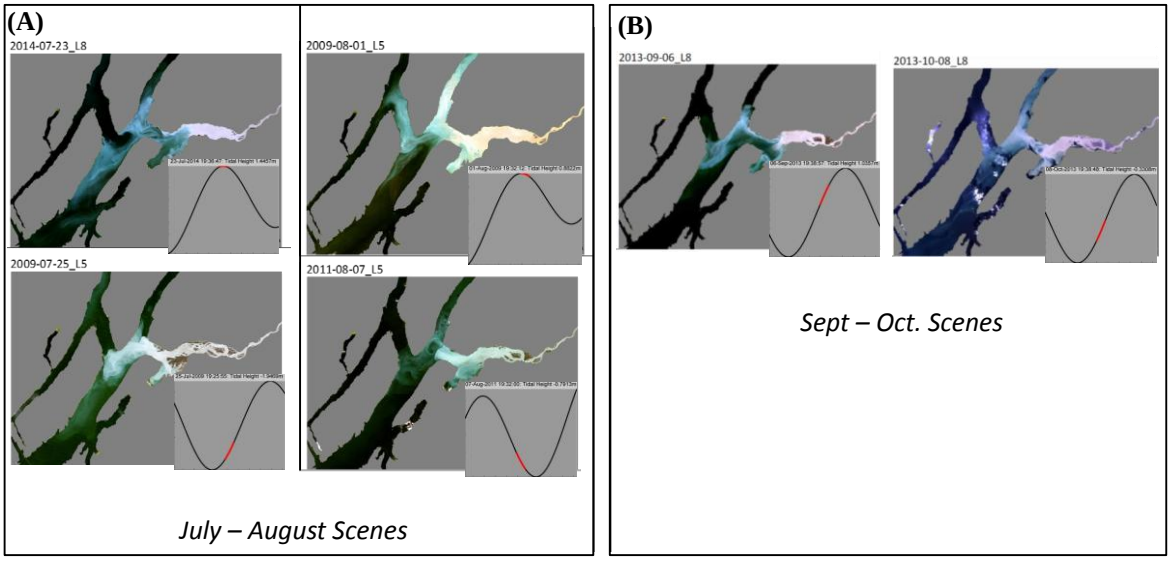

Figure 6. Landsat satellite imagery scenes of the Nass River plume (**A**) for July–August with moderate Nass River discharges and (**B**) for September–October with moderate to low river discharges for various years from 2008 to 2015. These RGB thumbnail images are uniformly enhanced using identical look-up tables. The top row of images are scenes during a flood tide and the bottom row of images are scenes during an ebb tide or at low water levels.

The 14 images of Figure 5 and Figure 6 are presented in order of the time of year, starting with an image from April 5, 2015 (Figure 5A) and ending with an image on October 8, 2013 (Figure 6B). In April, under very low Nass River sediment discharges, the Nass River plume is largely confined to upper Nass Bay with low levels of surface sediments extending into central Nass Bay and much lower sediment levels in Iceberg Bay as shown in Figure 5A. The surface sediments observed beyond Nass Bay in Portland Inlet and Observatory Inlet are generally low.

As the freshet begins in May and June (Figure 5B) and through July to early August (Figure 6A), the much larger sediment discharges from the Nass River result in distinct plume features extending beyond Nass Bay, to the south into Portland Inlet and to the north into Observatory Inlet. The location of the plume outside of Nass Bay is determined by the tidal currents, with flood currents resulting in a plume to the northeast in Observatory Inlet while ebb currents promote the plume moving to the southwest in Portland Inlet. During the peak discharges in mid- and late-May, a well-defined Nass River plume is evident extending to distances exceeding 40 km from the mouth of Nass Bay, especially to the south through Portland Inlet and to the north through the extension of Portland Inlet into Portland Canal. The northeastward extent of the plume in Observatory Inlet appears to be less than that of Portland Inlet, perhaps due to the net southwestward surface flow known to exist in the Observatory-Portland Inlet system (Pickard, 1961). From early August through to the fall months, the extent of the Nass River plume is reduced with the plume usually being evident in Portland Inlet and Observatory Inlet, but over distances limited to within about 10–15 km from the mouth of Nass Bay.

4. Oceanographic Regime of Nass Bay and Iceberg Bay: Forcing Mechanisms

The response of the circulation of the waters of Nass Bay and Iceberg Bay to physical forcing requires an understanding of these forcing mechanisms which can be derived from recent measurements. The major oceanographic forcing mechanisms in the Nass Bay area are the tidal currents and the freshwater discharges from the Nass River. Winds play a secondary role in terms of forcing of ocean currents.

4.1 Water Levels

The water levels on either side of the outer entrance to Nass Bay (Figure 2), were measured from August 3, 2015 to April 2, 2016. The full range of the water levels is 7.7 m which is nearly entirely due to the large tides in the region. The tides are dominated by the semi-diurnal tidal constituents (M2–78%, S2–9%, N2–6%, K2–0.6%) while the diurnal constituents (K1–6%, O1– 2%, P1–0.6%), contribute less than 9% of the total tidal height.

4.2 Ocean Currents

Ocean currents were measured at two ADCP mooring site locations, one in southern Nass Bay in 22 m water depth and the other in Iceberg Bay in 76 m water depth (Figure 2) over an eight-month period from August 2, 2015 to April 3, 2016. The measured currents in Nass Bay were much larger than those in Iceberg Bay. The average current speeds in Nass Bay were 17 cm/s at near-surface and 11 m depth, 16 cm/s at 19 m depth and 15 cm/s at 21 m depth. The corresponding maximum measured current speeds were 88, 103, 94 and 87 cm/s. By comparison, the average current speeds at the Iceberg Bay mooring were 6.1 cm/s at near-surface, 3.0 cm/s at 42 m depth, 3.5 cm/s at 66 m depth and 3.8 cm/s at 75 m depth. The maximum measured current speeds at the same depths were 39.8, 22.2, 18.1 and 17.6 cm/s. The reduced currents of Iceberg Bay are related to its much larger water depths compared to those of Nass Bay. In addition, Iceberg Bay is more isolated than Nass Bay from exchanges with other water bodies. In particular, this isolation is due to the greater separation between Iceberg Bay, by comparison with Nass Bay, to the inflowing Nass River water and the exchanges of waters into the estuary from the deeper waterways of Portland and Observatory Inlets. The numerical modeling results presented below provide further insights into the large differences between the circulation regime of Nass Bay and Iceberg Bay.

The larger currents in Nass Bay are dominated by the barotropic tidal current accounting for about 70% of the total variance of the ocean currents throughout the water column with the semi-diurnal tidal constituents being much larger than the diurnal tidal constituents. The Iceberg Bay currents are not only much weaker than those of Nass Bay, but also have baroclinic tidal currents being twice as large as the barotropic tidal currents. In fact, the barotropic tidal currents in Iceberg Bay are small being less than the variance contributed by sub-tidal currents, super-tidal currents as well as the larger baroclinic tidal currents.

4.3 Temperature, Salinity and Turbidity

During the 2015–2016 oceanographic measurement program, over 500 CTD-turbidity profile data sets were obtained in Nass Bay and Iceberg Bay at many locations throughout both of these Bays. These data sets are summarized as temperature-salinity diagram displays,

separately for Nass Bay (Figure 7A) and Iceberg Bay (Figure 7B). During the period of the July 20–22, 2015 measurements, when Nass River discharges are high, the water column is highly stratified with a wide vertical range in both temperature (14–8 ℃) and salinity (8 – <32 in Nass Bay; 12 – <32 in Iceberg Bay). The vertical gradients are most pronounced in the near-surface layer with the most intense halocline being at 2–3 m depth accompanied by a thermocline which extends to somewhat larger water depths of 5 m. As air and water temperatures cool and river discharge values decrease during the fall and winter, the observed ranges in temperature and salinity decrease and the water column becomes less stratified. During the time of fall measurements, October 28–30, 2015, the temperature range was reduced to only 2.0–2.5 ℃ while the salinity range was reduced from summer but still sizeable at 15 to 31–32 in both bays. By mid-winter, January 24–29, 2016, the range in water salinities were reduced even further to just 25 to 31–32. In winter, the surface temperatures are reduced to 4 ℃ which is well below the 7 ℃ water temperatures found in the lower part of the water column. The level of stratification in the water column is small compared to the summer. By early spring, March 31 to April 3, 2016, the temperatures begin to warm modestly although the measured temperature range is small, while the salinity range increased more than the increase in the temperature range to 19 to 31–32.

Turbidity values, also presented in Figure 5 and Figure 6, attain values of 10–15 NTU at near surface levels in summer and fall and while the turbidity is much lower in winter and early spring during the low Nass River discharges. In contrast, most of the turbidity measurements in the middle and deeper portions of the water column are well below 5 NTU throughout the year. Clearly, the near-surface turbidity and river discharge values are correlated over the seasonal cycle.

4.4 Winds

The winds blowing over the ocean waters of northern British Columba are affected by its location between the extensive network of mountainous islands separating the larger and more exposed outer Pacific Ocean waterways of Dixon Entrance and Hecate Strait to the west (Figure 1A), from the semi-enclosed, more sheltered inshore waters (Chatham Sound and Portland Inlet shown in Figure 1A) which are bordered on its east by the mountainous terrain of the mainland coast. The more open and exposed waterways to the west are dominated by the Pacific marine climate characterized by moderate air temperatures and intense storms in fall and winter (Fissel *et al.*, 2010). To the east, the temperatures exhibit a greater range, reflecting the increased influence of a continental climate. Here, the marine storm winds are generally abated by the mountainous terrain. In winter,

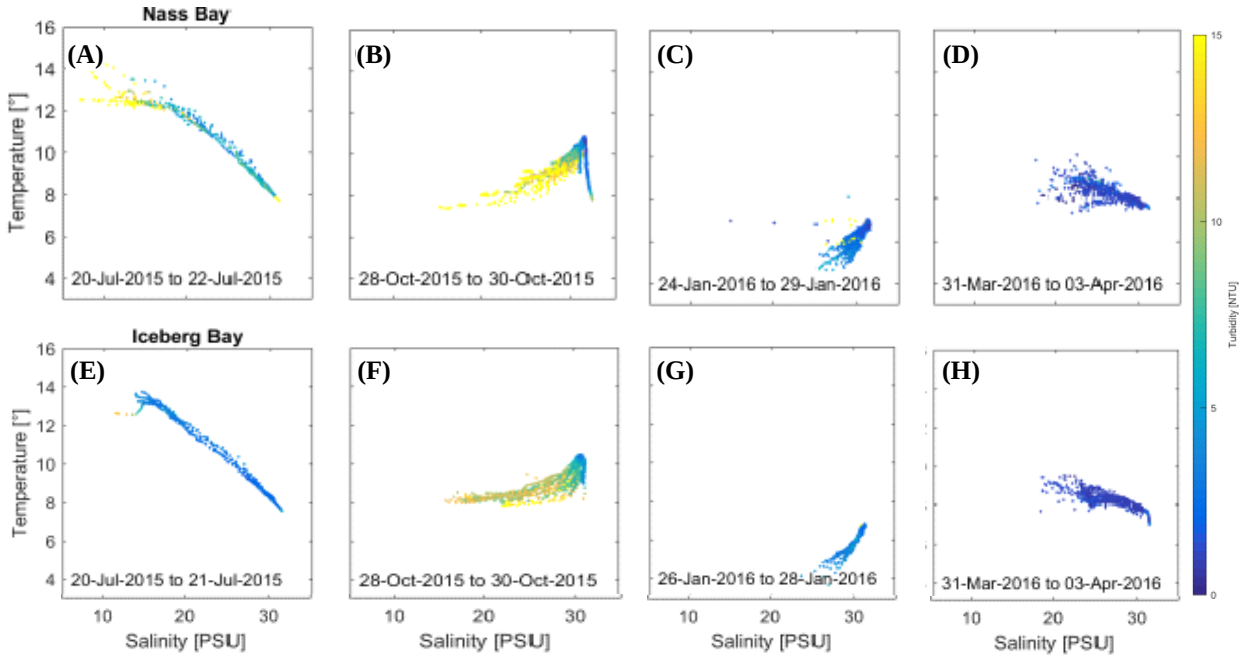

Figure 7. Temperature-salinity diagrams derived from CTD profiles collected in (**A–D**) Nass Bay and (**E–H**) Iceberg Bay during four sampling periods: July 20–22, 2015, October 28–30, 2015, January 24–29, 2016 and March 31–April 3, 2016. Turbidity was simultaneously measured and its values are shown by the colour coding as given in the scale on the right.

strong Arctic outflow winds occur as a result of the cold and dry continental Arctic high pressure system which episodically extends into the interior of British Columbia. The high atmospheric pressures in the interior can result in strong, low-temperature winds that flow into the inland fjords (Crawford *et al.*, 2007). These strong northeasterly winds can be accompanied by moderate to heavy snowfalls and squalls, and reduced visibility.

There are no direct measurements of winds in the study area. Model winds were used as sourced from Environment Canada's Meteorological Service (EC-MSC) using the High Resolution Deterministic Prediction System (HRDPS) (Mailhot *et al.*, 2014; https://weather.gc.ca/grib/grib2_HRDPS_HR_e.html). This system is comprised of a set of Limited Area Model (LAM) forecast grids with a 2.5 km horizontal grid spacing. The model outputs are improved from the original numerical weather prediction values by using observational inputs for clouds, precipitation and surface winds. The archived 10 m surface HRDPS wind speed and directions were acquired for the first five years in which these are available, spanning the years 2010 to 2015.

The HRDPS model winds were compared with observations at the nearest EC-MSC meteorological station located at Grey Islet (Figure 1A), located 55 km to the southwest of Nass Bay. This comparison of the observed and model winds revealed good agreement with a correlation score of better than 0.8. Here, the dominant Pacific coast cyclones resulted in prevailing southeasterly winds (from 135 °). Comparison of the prevailing wind directions between Nass Bay and Grey Islet showed notable differences. Nass Bay winds were generally directed from the east (from 90 °), particularly during high wind events which is attributable to topographic steering of the wind down the Nass River valley. This is most notable during winter when stable high pressure zones located over the interior of British Columbia and the Yukon Territory dominate the weather systems. Deep valleys, including the Nass River Valley, funnel wind down into the study region where the winds exit Nass Bay into Portland Inlet. Here the wind is funnelled down Portland Inlet to Grey Islet with prevailing winds from the northeast (40 °to 50 °).

Figure 8A presents the 2014–2015 wind speeds (blue line) along with the mean wind speeds for the five year period (red line) showing that the 2014–2015 winds are well above the five year mean values especially in the fall and winter. The five year mean winds are initially low, between 1 to 3 m/s from August to the end of September, then increase to mean values of 4 to 5 m/s later in the fall and early winter. In contrast, the 2014 winds reach speeds of 10 to 12 m/s for several days in December and a maximum of 16 m/s in January. The strongest winds are easterly, from 100 ° (Figure 8B), which is consistent with a winter high pressure dominating the area resulting in winds channelling down the valleys.

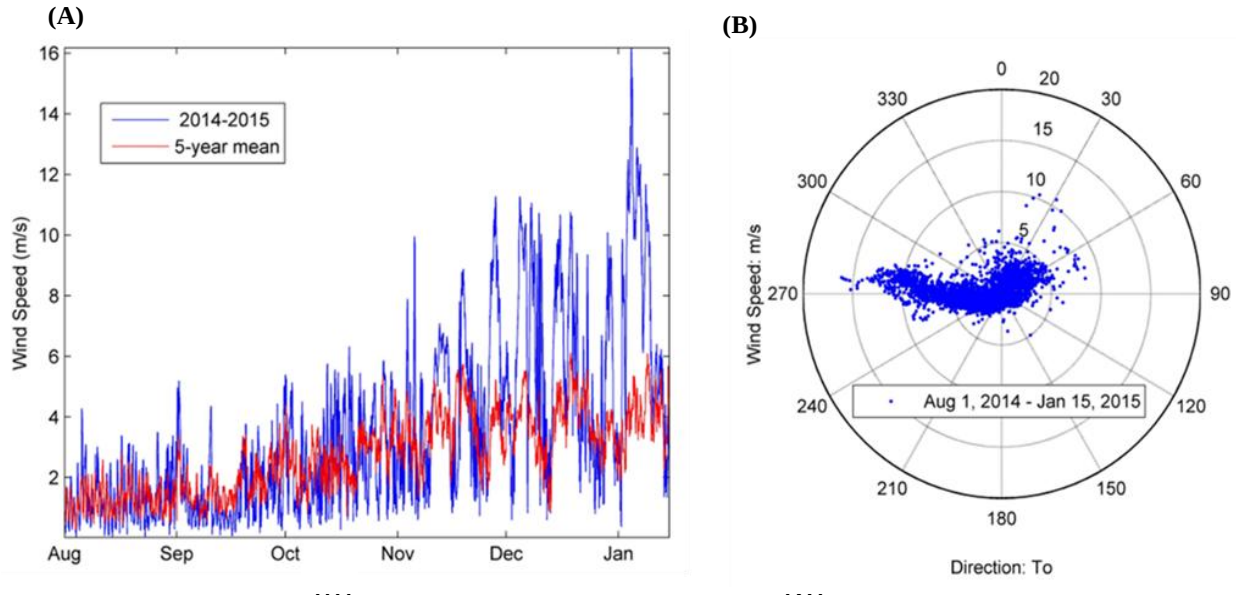

Figure 8. (**A**) Hourly winds obtained from Environment Canada's High Resolution Deterministic Prediction System (HRDPS) for August 2014 to January 2015 with wind speeds for this period compared to the five year mean speeds and (**B**) the directional distribution of wind speeds in Nass Bay.

5. Circulation Modeling of the Nass River Estuary

5.1 Model Setup

For this study, the Delft3D modeling system, an advanced suite of integrated numerical model modules, which can be combined with the Delft3D-Flow hydrodynamic model, was used to study the hydrodynamics and currents of the Nass River Estuary. The Delft3D model is widely used around the world in many applied projects and research studies (Deltares, 2015) including many hydrodynamic and sediment transport and fate studies for coastal waters. Delft 3D is one of a handful of advanced deterministic (process-based) coastal ocean models, which are routinely used for coastal hydrodynamic and sediment studies (Amoudry and Souza, 2011).

The model domain for the Nass River Estuary, comprised of Iceberg Bay and Nass Bay, is shown in Figure 2B. The northern open boundary, which is forced by the tidal heights, and the northeastern boundary, where the Nass River discharge is applied, are sufficiently distant from the main part of the model domain so as to not be affected by boundaries.

The single open boundary at the Nass Bay entrance to Portland Inlet is where tidal constituents are defined. Five major tidal height constituents (O1, K1, N2, M2, S2) were derived using tidal analysis methods (Foreman, 1977) from tide gauge data obtained from August 4th to October 31st, 2013 at the entrance to Nass Bay at the mouth of Portland Inlet near Gingolx (Figure 2B). The model open boundary at the Nass River mouth uses hourly river discharge data from the station "Nass River above Shumal Creek (08DB001)", operated by Environment Canada (Environment Canada, 2015) and available online at https:// wateroffice. ec. gc. ca/ report / data_ availability_e.html?type=historical&station=08DB001& parameter_type=Flow+and+Level.

Salinity conditions were required to initialise the model and provide the boundary conditions. These data were obtained using casts from a Conductivity Temperature Depth instrument (CTD) operated from August 3rd, 2015 across the mouth of Nass Bay and at multiple sites within Nass Bay and Iceberg Bay. The bathymetric data used as model input was obtained from Canadian Hydrographic Service (CHS) published chart (CHS Chart Number 3920–"Nass Bay, Alice Arm and Approaches") (Figure 2).

The horizontal model grid size is 35 m by 35 m, which provides a reasonably high-resolution in the horizontal while allowing for a realistic model run time. The number of sigma layers was set to 10. The relative layer depths from surface to bottom are 2%, 5%, 8%, 10%, 15%, 15%, 15%, 15%, 10%, and 5% of total water depths. These layers follow the bathymetry and allows adequate representation of the water column to ensure the surface and near bottom layer currents are captured in detail even in deep water grid locations.

5.2 Model Verification Run

Fieldwork carried out to characterize the study region provided verification data for the model. The modeled currents are compared with Acoustic Doppler Current Profiler (ADCP) mooring data located in Nass Bay (see Figure 2B) during a model verification run for a 25-day period in November 2015. The water depth of this mooring site is about 22.5 m. The model performance is verified against both surface (0.5 m below surface) and near-bottom (1 m above sea bed) current meter data. These comparative results for two levels are representative of the remainder of the water column.

The model was forced by the Environment Canada HRDPS gridded model winds for November 2015, having a spatial resolution of 2.5 km and a one-hour temporal resolution, and the tidal elevations at the open boundary. The tidal elevations at the open boundary is reconstructed based on the five major tidal height constituents (O1, K1, N2, M2, S2) derived using tidal analysis of water level measurements in Novmber 2015 (Foreman, 1977). There is a two-day spin up time after which time the model resulted in stable ocean currents. Then the model was integrated for 25 days in order to include both spring and neap tides. The model outputs were saved, as "snapshot" realizations, at 15-minute intervals. Hourly averaged velocities are used for comparison with the ADCP current data.

Comparisons of the modeled and observed near surface currents are shown in Figure 9. The model results and observations have very similar current speed distributions (Figure 9A). Both modeled and observed near surface speeds occur mainly within the range of 0.1−0.3 m/s. The model slightly overestimated the current speeds with about a 5% occurrence for large velocities over 0.4 m/s. Eastward (U, m/s) and northward (V, m/s) speed components are compared in Figure 9B and Figure 9C. The model reproduced the tidal cycle very well especially for the V component. Both model and observation show that the largest near surface currents are mainly directed towards the SSE flowing into the shallow portions of southern Nass Bay. The differences between spring and neap near surface tidal currents for the smaller U component is relatively larger than for the V component, especially during the period of spring tidal flows. For the larger V component, the fortnightly tidal

cycle exhibits large changes in the near-surface current from 0.2 m/s at neap tides to 0.5 m/s at spring tides, with a distinct asymmetry toward larger southerly (negative) values evident in both the model and observed currents. The root-mean-square deviation (RMSD) values for the U and V components are 0.16 and 0.14 m/s, respectively.

The near-bottom currents are weaker than the near-surface currents with speeds ranging from 0–0.2 m/s (Figure 10A). The distribution of the model-derived near-surface current speeds show good agreement in near-bottom current speeds. RMSD values for U and V components (Figure 10B and Figure 10C) are 0.08 and 0.07 m/s in the model. The spring and neap tidal currents have smaller differences in the V component by comparison to the near-surface flow, which is indicative of the vertical stratification in the tidal current fields from the surface to near-bottom at the location of the ADCP site. Overall, the model results show good agreement with observations.

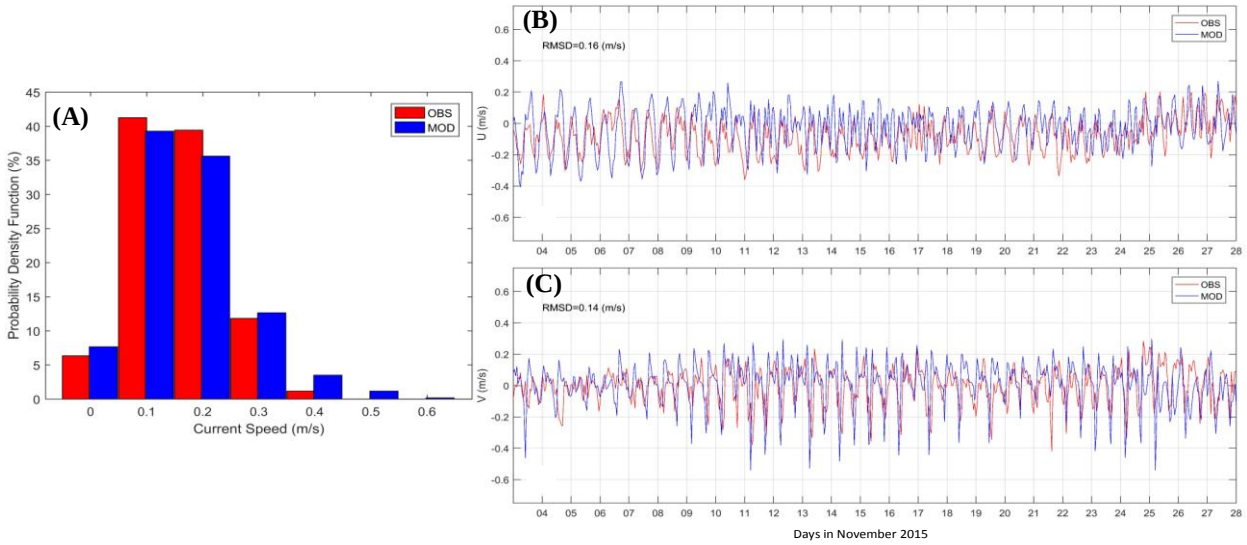

Figure 9. Comparison of modeled (blue) and observed (red) near-surface currents (hourly, 0.5 m below surface) during the verification run of November 3–27, 2015 at ADCP mooring site (as marked in Figure 2). (**A**) Current speed histogram; Time series of (**B**) easting (u) and (**C**) northing (v) components as well as the root-mean-square difference (RMSD) values between the model and observations for u and v.

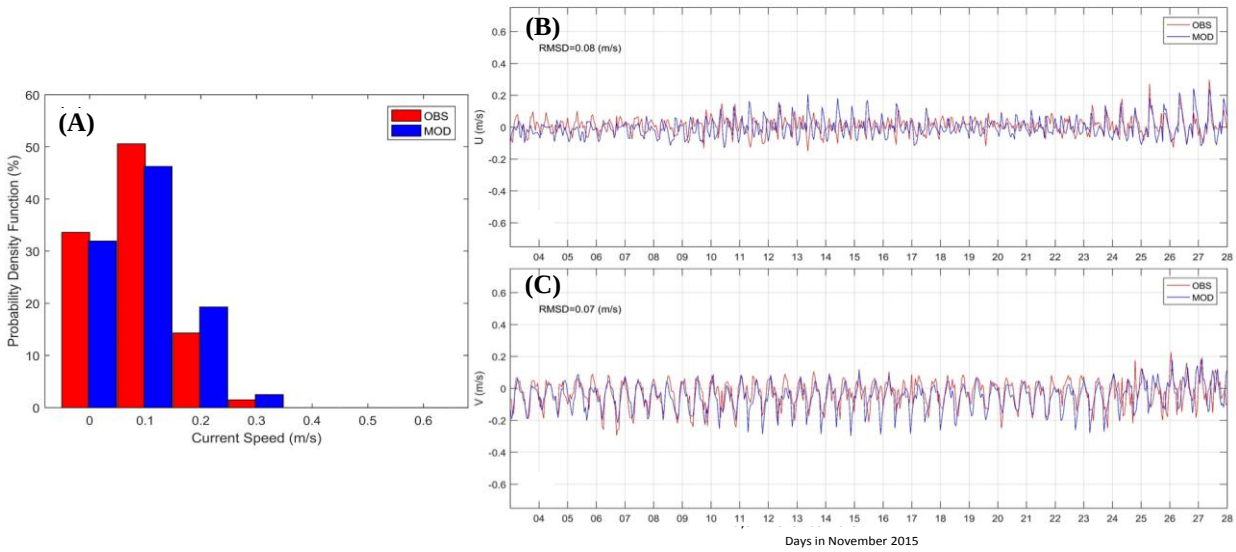

Figure 10. Comparison of modeled (blue) and observed (red) near-bottom currents (hourly, 0.5 m below surface) during the verification run of November 3–27, 2015 at ADCP mooring site (as marked in Figure 2). (**A**) Current speed histogram; Time series of (**B**) easting (u) and (**C**) northing (v) components as well as the root-mean-square difference (RMSD) values between the model and observations for u and v.

5.3 Model-derived Tidal Current Flows in Nass Bay and Iceberg Bay

The Delft3D numerical model was used to simulate the tidal current patterns in Nass Bay and Iceberg Bay under different stages of the tidal cycle and Nass River freshwater discharges. The model was run over a four-month period (August 1–November 30, 2017) with model outputs saved every 1.5 hours. Winds for this August to November period were chosen to be those available for 2014 because this year had the largest wind speeds for the five years of wind data available. For consistency, the hourly Nass River discharge is taken from the same period over which time Nass River discharges have an observed range of values of 120–2873 m^3/s. The salinity profile is representative of the initial conditions and tidal heights at the open boundary were computed from tidal analysis prediction (Foreman, 2007) of water level measurements obtained in 2015–2016 for the August–November 2017 model run.

The model results show that the Nass Bay tidal currents have complex spatial patterns (Figure 11 and 12). As shown in Figure 11, during the flood tidal flows, both strong surface and near bottom tidal currents occur laterally flowing to the northeast across Nass Bay in bands along the deeper waters of the northern side and along the southeast shoreline. The tidal flow bifurcates into two branches, one to the north directly into the Nass River estuary and the other, mainly for near the surface, to the southeast over and around the shallow Nass Bay tidal flats. On the other hand, the inflow currents into Iceberg Bay occur mainly in the deeper portion of the water column. The surface flow speeds in Iceberg Bay are much weaker than the surface flows in Nass Bay.

During ebb tide (Figure 12), strong currents are present along the northern part of Nass Bay as a combination of the tidal currents and outflow from the Nass River. The outflow currents also extend into southeastern Nass Bay as a nearshore current in the shallow waters and then exits the bay through the western side of the Nass Bay entrance.

5.4 Distribution of Bottom Shear Stress

Modeled bottom shear stress is analyzed in this section. A four month-model run (August to November) was made over a period of variable Nass River discharges (120–2873 m^3/s), relatively low and high seasonal winds, and spanning eight fortnightly tidal cycles (see Figure 13).

The model results presented here are for the same forcing conditions as applied in Section 5.3. Episodic occurrences of large bottom currents and bottom shear stress are seen in the model results. During spring tide, in the near-bottom model layer just above the seabed, the model simulates erosion of deposited sediments which result in episodic occurrences of high total suspended sediment (TSS) levels. The distribution of bottom shear stresses in time and space provides important perspectives for us to better understand the sediment transport processes in Nass Bay and Iceberg Bay, in addition to the satellite images which are limited to the surface layer.

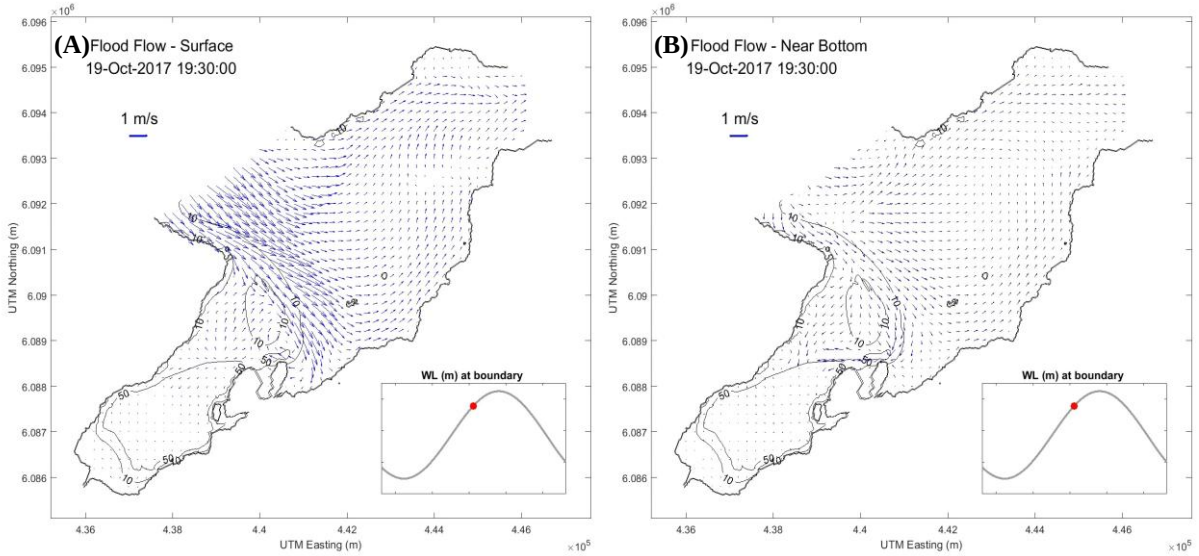

Figure 11. Numerical model results showing the (**A**) surface and (**B**) near bottom currents in Nass Bay and Iceberg Bay for flood flows. The water level at the time of the model results are shown in the small inset box in each panel.

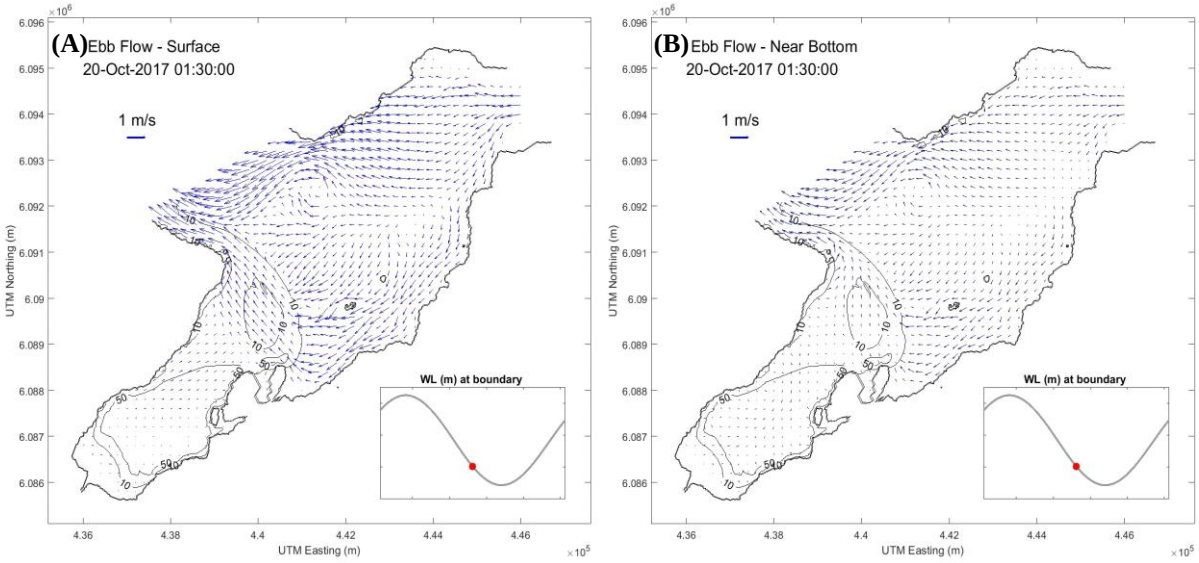

Figure 12. Numerical model results showing the (**A**) surface and (**B**) near bottom currents in Nass Bay and Iceberg Bay for ebb flows. The water level at the time of the model results are shown in the small inset box in each panel.

Time series of model-derived bottom shear stresses in Nass Bay and Iceberg Bay, averaged over the full model domain, is shown in Figure 13A. Also shown are the Nass Bay wind speeds for central Nass Bay (Figure 13B), domain-averaged water levels (Figure 13C), and the Nass River freshwater discharges (Figure 13D). The results show that the bottom shear stress levels are dominated by tidal currents. The role of the surface winds is of minor importance as indicated in Figure 13. However, enhanced and reduced stratification associated with the freshwater discharges from the Nass River is expected to influence the bottom shear stress for specific locations.

Figure 14 shows the distribution of median values in time for bottom shear stresses in Nass Bay and Iceberg Bay (Figure 14A) based on model results from August to November. Large bottom stress values occur laterally from the western end of Nass Bay across to the entrance to Nass Bay. Large bottom shear stresses also occur along the eastern entrance to the Bay and extending to the southern shoreline of Nass Bay, which is corresponds to the strong tidal flow areas as shown in Figure 11 and 12.

Correlation coefficients are calculated, between time series of bottom shear stresses and water levels at every model grid as presented in Figure 13. Since the tides are dominated by the M2 tidal constituents, with the M2 tidal heights accounting for 78% of the total tidal heights derived from all tidal constituents, the time series of water levels have been shifted 3.1 hours earlier so that the positive peaks in the shifted time series are actually representing maximum flood flow, and the negative peaks appear to be associated with maximum ebb current speeds. The correlation coefficient map is shown in Figure 14D. Red areas (positive correlation coefficients) indicate the correlation between the local bottom shear stresses and flood flow, while the blue areas (negative correlation coefficients) identify the locations where bottom shear stresses are more affected by ebb flow. The distribution features are consistent with the near-bottom flow pattern demonstrated in Figure 12 and confirm that the tidal currents are the dominant factor for generating the large bottom shear stresses (and associated erosion). The positive correlation values at the entrance to Iceberg Bay indicate the strong bottom flow in Iceberg Bay mainly occur during flood periods. The negative (blue) area over the Nass Bay tidal flats demonstrate that the large bottom shear stress here is associated with high water turning to ebb flows, because high water level is needed to provide strong flow over this shallow area.

Figure 14B plots the map of correlation coefficients between the bottom shear stress and the absolute values of the 3.1 hour shifted water levels relative to mean water level, *i.e.* as a scalar representation of water levels about their mean values. In this correlation coefficient map, large positive values represent areas where the tidal currents are dominant in determining the bottom shear stress, which includes virtually all of Nass Bay. In contrast, Iceberg Bay has small correlation coefficients

of the bottom shear stress to the scalar version of time shifted water levels which is indicative of processes other than tidal currents being important to the bottom shear stress regime of Iceberg Bay.

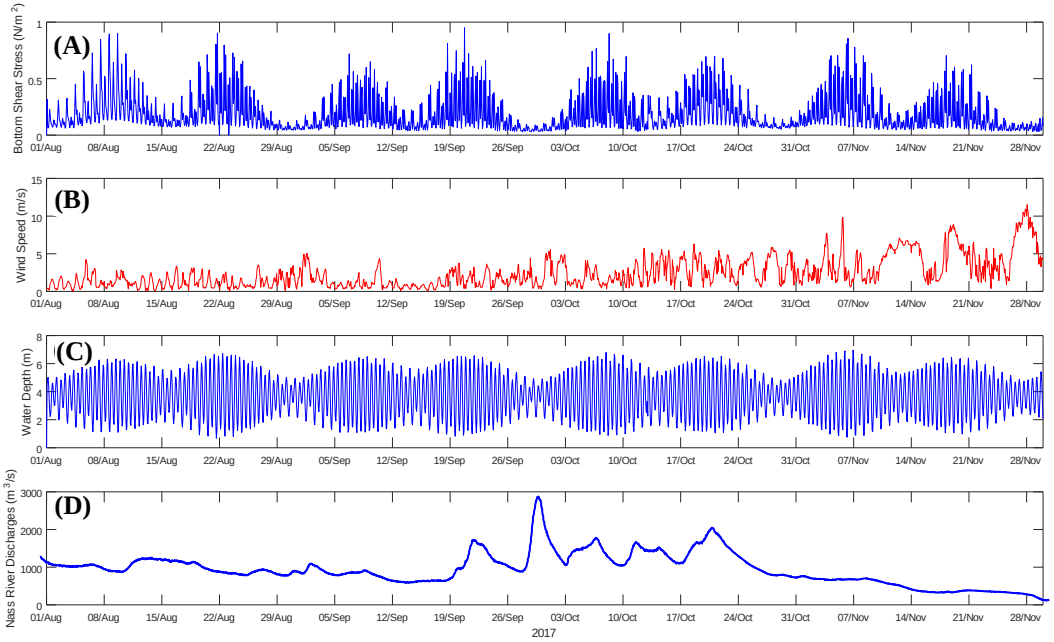

Figure 13. Time series plots of (**A**) the model-derived bottom shear stresses averaged over Nass Bay and Iceberg Bay at 1.5 hour intervals from August 1 to November 30, 2017. Also shown are (**B**) the wind speeds in central Nass Bay, (**C**) averaged water levels, and (**D**) the Nass River freshwater discharges during the model integration period.

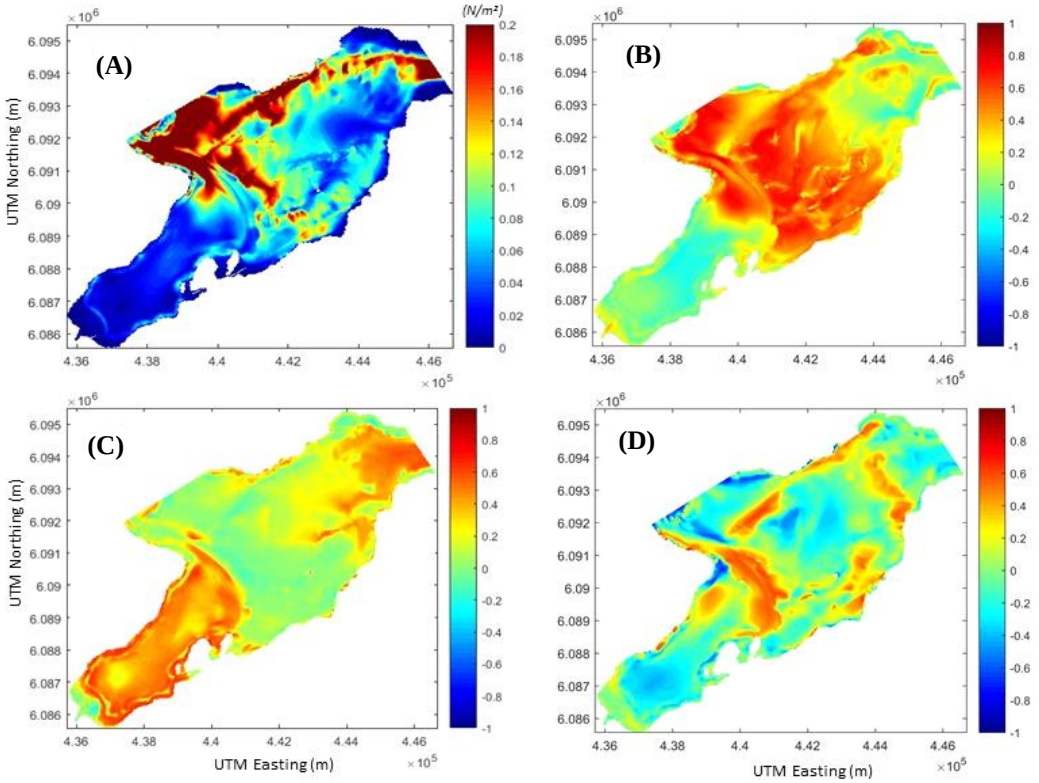

Figure 14. (**A**) Median values of bottom shear stresses (BSS) in Nass Bay and Iceberg Bay based on model results from August 1 to November 30, 2017. (**B**) Correlation coefficients between time series of BSS and absolute values of water level anomalies (shifted 3.1 hours earlier). (**C**) Correlation coefficients between 30-day low-pass filtered time series of BSS and the Nass River freshwater discharges (shifted 20 days earlier). (**D**) Similar to (**B**) but with different water level anomalies (shifted 3.1 hours earlier, positive to negative anomalies).

Figure 14C shows correlation coefficients between 30-day low-pass filtered time series of bottom shear stresses and the Nass River freshwater discharges. The time series of filtered Nass River discharges have been shifted 20 days earlier, in order to consider the time lag between the freshwater discharge and the near bottom flow changes (river discharges leading). Significant correlation values are found at the Nass River Estuary, where the river discharges directly influence the flow regime. Another important finding is the significant correlation values covering the entirety of Iceberg Bay, where the tidal currents are much weaker than those of Nass Bay. The variability of the near bottom flow/shear stress in Iceberg Bay is significantly affected by Nass River freshwater discharge variations.

6. Summary and Conclusions

The Nass River Estuary exhibits dynamic and complex flow patterns. The complexity of the flow patterns is associated with: the small along-inlet distance of Nass Bay relative to the larger cross-inlet lateral distance (Nass Bay and Iceberg Bay); the highly stratified waters undergoing large seasonal variability; combined with the very large tides in this region.

The Nass River plume impacts adjoining waterways well beyond the local receiving water bodies of Nass Bay and Iceberg Bay. Based on an analysis of Landsat satellite imagery data sets from 2008–2015, it was shown the Nass River suspended sediment plume can extend more than 40 km from Nass Bay, under freshet river flows in late spring and summer and during episodic large rainfall events in fall.

Using direct measurements and 3D numerical modeling of the ocean circulation, large tidal currents occur in Nass Bay, attaining maximum speeds of just over 1 m/s. The tidal currents in Nass Bay have complex spatial patterns with the largest ebb tidal currents being directed from west to east through the northern half of the entrance to Nass Bay and a weaker secondary ebb tidal flow into southern Nass Bay and then exiting on the southeast side of the Nass Bay entrance. On the flood tide, strong tidal currents enter Nass Bay on its eastern side and bifurcate into a branch moving westward and a branch continuing to the southwest and travelling westward along the southern shore.

The ocean current speeds in Iceberg Bay are considerably smaller due to the notably larger water depths and the greater distance from the Nass River flows into the eastern end of Nass Bay and location of Iceberg Bay. Iceberg Bay has a higher degree of water column stratification than Nass Bay, especially in the fall, and tends to have a more baroclinic or internal tidal flow regime than Nass Bay. Near-bottom currents on the flood tide are larger than for the ebb tide at the entrance to Iceberg Bay which may bring more saline and colder water into Iceberg Bay *via* the eastern entrance to Nass Bay.

Detailed model simulations of the 3D circulation in Nass Bay and Iceberg Bay over a four-month period from August to November, representative of wind and river forcing for the year 2014 and tidal forcing for the year 2017, were used to examine the principal forcing mechanisms of the study area. From an analysis of the model-derived bottom shear stress values, it was shown that tidal currents are dominant in nearly all of Nass Bay in generating the bottom shear stress with large peak shear stress values occurring during the spring tides. The imbalance between flood and ebb bottom tidal flows is evident in the eastern portion of Nass Bay and along the southern shoreline of Nass Bay where flood tidal current speeds are much larger than those of the ebb tidal currents. In contrast, the ebb tidal currents dominate over the flood tidal currents in western Nass Bay and in the central and northern portions of the entrance to Nass Bay. The correlation between bottom shear stress and the 20-day lagged Nass River discharge reveals that the River discharge is important to driving bottom shear stress in the westernmost part of Nass Bay, where the River waters enter the Bay and also in the bottom shear stresses of Iceberg Bay.

The Nass River tidal estuary consists of Nass Bay, and the laterally adjoining Iceberg Bay which has much deeper waters than Nass Bay. This estuary is unusual compared to more traditional tidal estuaries which can be characterized by the two dimensions of the along-inlet in the horizontal and depth in the vertical. The complex three-dimensional exchanges between Nass Bay and Iceberg Bay warrant further study.

Acknowledgements

We thank our colleagues at ASL Environmental Sciences Inc. for their contributions to this study, in particular to James Bartlett who conducted the *in-situ* oceanographic data collection under the direction of Todd Mudge. We also thank the reviewers of this journal whose comments led to substantial improvements to this paper.

References

Amoudry L O, Souza A J. (2011). Deterministic coastal morphological and sediment transport modeling: A review and discussion. *Reviews of Geophysics*, 49(2): RG2002. https://dx.doi.org/10, 1029/2010RG000341

Birch J R, Luscombe E C, Fissel D B, *et al.* (1985). West coast data inventory and appraisal. *Canadian Data Report of Hydrography and Ocean Sciences*, 1(37): 302. Department of Fisheries and Oceans, Institute of Ocean Sciences, Sidney, BC, Canada.

Canadian Hydrographic Service (CHS). http://www.charts.gc.ca, accessed June 2017

Constantin S, Doxaran D, Constantinescu S. (2016). Estimation of water turbidity and analysis of its spatio-temporal variability in the Danube River plume (Black Sea) using MODIS satellite data. *Continental Shelf Research*. 112(2016): 14–30. https://dx.doi.org/10, 1016/j.csr, 2015, 11.009

Crawford W, Johannessen D, Whitney F, *et al.* (2007). Appendix C: Physical and chemical oceanography. In Ecosystem overview: Pacific north coast integrated management area (PNCIMA). Lucas B G, Verrin S, and Brown R (editors). *Canadian Technical Report of Fisheries and Aquatic Sciences*. 2667: 7, 77.

Chen Z, Hu C, Muller-Karger F. (2007). Monitoring turbidity in Tampa Bay using MODIS/Aqua 250-m imagery. *Remote Sensing of Environment*, 109(2): 207–220. https://dx.doi.org/10, 1016/j.rse, 2006, 12.019

Deltares. (2015). Software simulation products and solutions [Internet]. www.deltares.nl/en/software- solutions/

Environment C. (2015). Hydrometric data and information service: Service standards [Internet]. https://wateroffice.ec.gc.ca/

Farmer D M, Denton R A. (1985). Hydraulic control of flow over the sill of observatory inlet. *Journal of Geophysical Research Oceans*, 90 (C5): 9051–9068. https://dx.doi.org/10, 1029/JC090iC05p09051

Fissel D B, Borg K, Lemon D, *et al.* (2010). Technical data report: Physical marine environment, enbridge northern gateway project [Internet]. http://www.northerngateway.ca/assets/pdf/tdr/Risk%20Technical%20Data%20Reports/Marine%20Physical%20Environment_TDR.pdf

Foreman M G G. (1977). Manual for tidal heights: Analysis and prediction. *Pacific Marine Science Report*, 97: 1–66. https://dx.doi.org/10, 1007/BF02692224

Gholizadeh M H, Melesse A M, Reddi L. (2016). A comprehensive review on water quality parameters estimation using remote sensing techniques. *Sensors*, 16(8): 1298. https://dx.doi.org/10.3390/s16081298

Krauel D P. (1981). Deep water flow and exchange processes in Alice Arm B.C. Woodward-clyde consultants for environmental protection service environment Canada, west vancouver, B.C [Internet]. http://www.dfo-mpo.gc.ca/library/61214.pdf

McKee C. (2010). *Treaty talks in British Columbia*. Canada: University of British Columbia Press.

Mailhot J, Milbrandt J A, McTaggart-Cowan R, *et al.* (2014). An experimental high-resolution forecast system during the Vancouver 2010 winter olympic and paralympic games. *Pure & Applied Geophysics*, 171(1–2): 209–229. https://dx.doi.org/10, 1007/s00024-012-0520-6

Miller R L, McKee B A. (2004). Using MODIS Terra 250m imagery to map concentrations of total suspended matter in coastal waters. *Remote Sensing of Environment*, 93(1): 259–266. https://dx.doi.org/10, 1016/j.rse, 2004.07.012

Pickard G L. (1961). Oceanographic features of inlets in the British columbia mainland coast. *Journal of the Fisheries Research Board of Canada*, 18(6): 907–999. https://dx.doi.org/10, 1139/f61-062

Quang N H, Saski J, Higa H, *et al.* (2017). Spatiotemporal variation of turbidity based on landsat 8 OLI in cam ranh bay and thuy trieu lagoon, Vietnam. *Water*, 9(8): 570. https://dx.doi.org/10.3390/w9080570

Stacey M W, Zedel L J. (1986). The time-dependent hydraulic flow and dissipation over the sill of observatory inlet. *Journal of Physical Oceanography*, 16(16): 1062–1076. https://dx.doi.org/10, 1175/1520-0485(1986)016<1062:TTDHFA> 2.0.CO;2

Sierra Club of Canada. (2006). Nass River salmon fishery report card [Internet]. http://www.sierraclub.ca/national/postings/scc-nass-salmon-report-card.pdf

United States Geological Survey (USGS). (2016). Landsat 8 (L8) data users handbook [Internet]. https://landsat.usgs.gov/landsat-data-access

United States Geological Survey (USGS). (2017). Landsat data access [Internet]. https://landsat.usgs.gov/landsat-data-access